Monte Carlo simulation based study of a proposed multileaf collimator for a telecobalt machine

G. Sahani[a)]
Radiological Safety Division, Atomic Energy Regulatory Board, Anushaktinagar, Mumbai-400094, India

Sunil Dutt Sharma
Radiological Physics and Advisory Division, Bhabha Atomic Research Centre, CT & CRS, Anushaktinagar, Mumbai-400094, India

P. K. Dash Sharma
Radiological Safety Division, Atomic Energy Regulatory Board, Anushaktinagar, Mumbai-400094, India

D. N. Sharma
Health Safety and Environment Group, Bhabha Atomic Research Centre, Trombay, Mumbai-400085, India

S. A. Hussain
Radiological Safety Division, Atomic Energy Regulatory Board, Anushaktinagar, Mumbai-400094, India

Purpose: The objective of the present work was to propose a design of a secondary multileaf collimator (MLC) for a telecobalt machine and optimize its design features through Monte Carlo simulation.
Methods: The proposed MLC design consists of 72 leaves (36 leaf pairs) with additional jaws perpendicular to leaf motion having the capability of shaping a maximum square field size of 35×35 cm^2. The projected widths at isocenter of each of the central 34 leaf pairs and 2 peripheral leaf pairs are 10 and 5 mm, respectively. The ends of the leaves and the x-jaws were optimized to obtain acceptable values of dosimetric and leakage parameters. Monte Carlo N-Particle code was used for generating beam profiles and depth dose curves and estimating the leakage radiation through the MLC. A water phantom of dimension $50 \times 50 \times 40$ cm^3 with an array of voxels ($4 \times 0.3 \times 0.6$ cm^3 $= 0.72$ cm^3) was used for the study of dosimetric and leakage characteristics of the MLC. Output files generated for beam profiles were exported to the PTW radiation field analyzer software through locally developed software for analysis of beam profiles in order to evaluate radiation field width, beam flatness, symmetry, and beam penumbra.
Results: The optimized version of the MLC can define radiation fields of up to 35×35 cm^2 within the prescribed tolerance values of 2 mm. The flatness and symmetry were found to be well within the acceptable tolerance value of 3%. The penumbra for a 10×10 cm^2 field size is 10.7 mm which is less than the generally acceptable value of 12 mm for a telecobalt machine. The maximum and average radiation leakage through the MLC were found to be 0.74% and 0.41% which are well below the International Electrotechnical Commission recommended tolerance values of 2% and 0.75%, respectively. The maximum leakage through the leaf ends in closed condition was observed to be 8.6% which is less than the values reported for other MLCs designed for medical linear accelerators.
Conclusions: It is concluded that dosimetric parameters and the leakage radiation of the optimized secondary MLC design are well below their recommended tolerance values. The optimized design of the proposed MLC can be integrated into a telecobalt machine by replacing the existing adjustable secondary collimator for conformal radiotherapy treatment of cancer patients. © *2013 American Association of Physicists in Medicine*. [http://dx.doi.org/10.1118/1.4773308]

Key words: MLC, Monte Carlo, dosimetry, leakage

I. INTRODUCTION

Telecobalt machines and medical linear accelerators (linacs) were introduced simultaneously in the early 1950s and emerged as competitive technologies for the external beam therapy (EXBT).[1] A number of advancements have taken place in linacs whereas modernization of telecobalt machines has been almost negligible. For example, commercial telecobalt machine is yet to be augmented with a multileaf collimator (MLC), which is a necessary element for efficient delivery of conventional three-dimensional conformal radiation therapy (3D-CRT) and a basic requirement for the implementation of intensity modulated radiation therapy (IMRT).[2,3] As a result, by the 1990s telecobalt based EXBT had fallen from favor in the developed countries like the United States.[1,4] A few investigators have carried out feasibility studies toward modernizing telecobalt machine as a tomotherapy device.[2,3,5] Joshi *et al.*[2] investigated tomotherapy dose distributions for

two clinical cases by comparing ^{60}Co based tomotherapy and a 6 MV linac based tomotherapy. They demonstrated that ^{60}Co based tomotherapy dose distributions were comparable to 6 MV linac based tomotherapy. Schreiner *et al.*[3] reported that telecobalt machine can be used as an image guided radiation therapy (IGRT) device. Adams and Warrington[6] executed conformal radiation therapy and IMRT treatment plans created for ^{60}Co using blocks and compensators for a range of treatment sites and compared them with those created using 6/10 MV photons with a MLC. They found that the treatment plans using ^{60}Co beam and 6/10 MV photon with a MLC were comparable to each other for the same site. However, implementing conformal radiation therapy/IMRT with blocks or compensators is a laborious process. Thus, there is a need to design and develop a MLC for a telecobalt machine for upgrading it as a conformal dose delivery device.

It is worth mentioning that the majority of radiotherapy centers in developing countries use telecobalt machines for cancer treatment and is preferred over medical linacs because of: (i) low purchase and maintenance cost, (ii) lower power requirements, and (iii) less down time, even though the medical linac is advantageous over telecobalt machine in various aspects such as variable dose rates, multiple photon and electron beam energies, and smaller beam penumbra.[7,8] Telecobalt machines use either multivane or jaw type collimator system to vary the size and shape of the radiation beam.[9,10] With the current collimating assembly a telecobalt machine can define either square or rectangular treatment fields only. Since tumors are of irregular shapes and sizes, irradiation of healthy tissues surrounding the tumor in the field defined by the multivane or jaw type of collimator is inevitable. Replacement of secondary collimator (multivane or jaw type) by the MLC in a telecobalt machine will also eliminate the necessity of fabricating individualized shielding blocks required for defining irregular fields. Sahani *et al.*[7] has reported that telecobalt machine having jaw type secondary collimator (adjustable collimator) could be augmented with MLC. A cerrobend based prototype tertiary MLC for telecobalt machine was proposed by Singh *et al.*[11] which can define the maximum field size of 13.4×13.4 cm^2. This MLC is made up of a cerrobend material which has limited durability and mechanical limitation in its smooth routine use. Ayyangar *et al.*[12] also proposed a design of a tertiary MLC for telecobalt machines which can define field sizes of up to 20×20 cm^2. In addition, the designs of the MLCs proposed by these authors will add additional weight to the head of the telecobalt unit, which may affect the isocentric accuracy. It is required to propose an optimized design of a secondary MLC free from these limitations, which can easily be fabricated and augmented with the existing telecobalt machines. In this work, a 72 leaves (36 pairs) MLC is proposed and Monte Carlo simulation of this MLC is conducted to optimize the design parameters. The dosimetric characteristics and radiation safety related parameters of the proposed MLC assembly are evaluated through Monte Carlo simulation. This paper describes in detail the Monte Carlo simulation of the design aspects, dosimetric characteristics, and radiation leakage characteristics of the proposed MLC.

II. MATERIALS AND METHODS

II.A. Monte Carlo method

The Monte Carlo N-Particle transport code (MCNP) version 4B was used in this study. MCNP4B is a general purpose continuous energy generalized geometry and time dependent code, which deals with the transport of neutrons, photons, and coupled electron photon transport, i.e., transport of secondary electrons resulting from gamma interactions.[13] The code was run in the combined photon electron mode. As low energy particles in energy deposition tallies make little contribution, 0.01 MeV for photon and 0.1 MeV for electron were chosen as cutoff energies[14–17] to reduce the computational time without compromising the accuracy of the simulation. *F8 tally (pulse-height distribution tally modified to energy units) was used to score energy deposited in MeV in each voxel per source particle.

MCNP4B has the ability to fully describe a single (or few) MLC leaf as a cell, then using cell transformations (rotations and translations) to specify additional MLC leaves. The above code was used for the transport of radiation through the source capsule, telecobalt head, primary collimator, MLC, x-jaws, and phantom. A stainless steel encapsulated source with an active cylindrical ^{60}Co source of 2 cm diameter and 2 cm height was used in the simulation. The encapsulated ^{60}Co source contains a large number of cylindrical pellets (typically 1 mm diameter and 1 mm height). Due to the presence of air gaps among the pellets the effective density of the encapsulated ^{60}Co source reduces to about 5.4 g/cc (known as packing density of the source).[18,19] This packing density of the source was considered in our simulation. A water phantom of dimension $50 \times 50 \times 40$ cm^3 having array of 0.72 cm^3 voxels were used in simulation for determining dose distribution. The dimension of each voxel is $4 \times 0.3 \times 0.6$ cm^3, where 0.3 cm is the voxel width along x/y-axis corresponding to x/y-profile and 4 cm is the voxel length perpendicular to the x/y-axis, and 0.6 cm is the voxel height along z-axis. The energy deposited in voxels was scored per source particle for the study of dosimetric and leakage characteristics of the MLC. MCNP input file was run up to 10^9 histories. Beam profiles in all the studies were generated at the depth of dose maximum (d_m) with source to surface distance (SSD) of 79.5 cm. Figure 1 is the schematic diagram of the geometry used in the Monte Carlo simulations.

II.B. Benchmarking of the simulation

To benchmark the accuracy of the Monte Carlo simulation, experimentally measured dosimetry data of the Bhabhatron-II telecobalt machine were compared with the Monte Carlo generated data. The existing design of the Bhabhatron-II telecobalt machine was modeled and the Monte Carlo generated profiles and depth dose curves compared with measured data. The Bhabhatron-II telecobalt machine uses jaw type of adjustable collimators (secondary collimator) with trimmer bars, which follows the jaws in order to reduce the magnitude of radiation beam penumbra. In this machine, adjustable collimators including trimmers are aligned to match with the
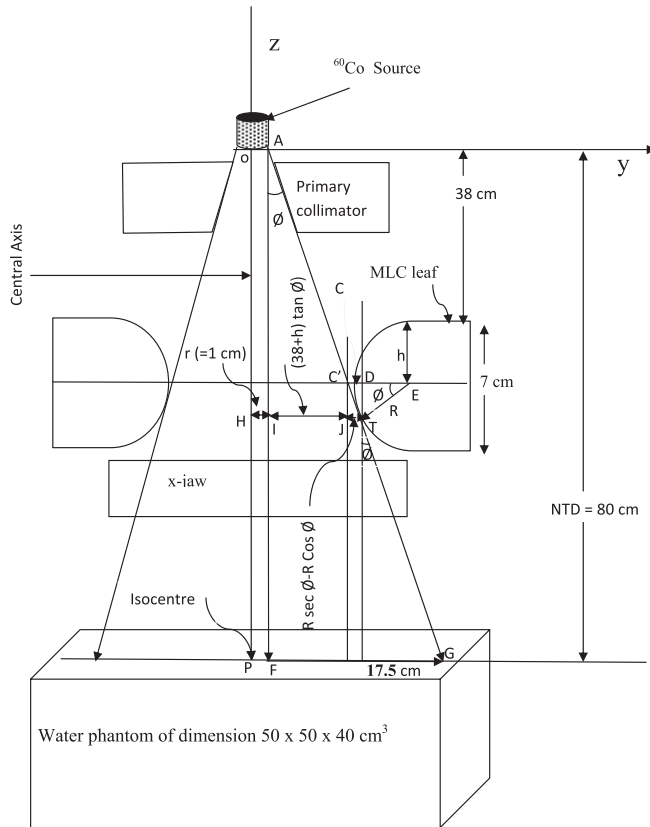
FIG. 1. Schematic diagram showing dimensional details of the water phantom, MLC leaves, and location of the MLC with respect to the source bottom. T is the point located on the leaf end at the tangent (AG) drawn from the periphery of source bottom. R is the radius of curvature of the leaf end and h is the distance of center of curved leaf end from the top of the leaf. This geometry was used in Monte Carlo simulation.

beam divergence. Beam profiles and depth dose curve for 10×10 cm^2 open beam were generated through Monte Carlo simulation and measured data obtained using the PTW radiation field analyzer (RFA). Beam profiles output files generated by MCNP4B were exported to the PTW beam analyzer software through locally developed software in Pascal using Delphi 6.0 (Borland Software Corporation, Scotts Valley, CA) in order to evaluate radiation field size, beam flatness, symmetry, and penumbra.

II.C. Basic design of the MLC

The basic design of the MLC which was evaluated through Monte Carlo simulation consists of 72 leaves (each of height 7.0 cm with rounded end) with additional jaws perpendicular to leaf motion. This MLC can define maximum square field of 35×35 cm^2 and irregular field sizes as per clinical requirements. A distance of 45 cm between the source bottom and the bottom of the MLC and 51 cm between the source bottom and the bottom of the x-jaws (perpendicular to leaf motion) were chosen to minimize the magnitude of radiation beam penumbra while maintaining sufficient clearance between the bottom of the collimating system and the isocenter. The adjustable collimator of current telecobalt machines can define

a maximum field size of 35×35 cm^2. This traditional requirement was carried forward in the proposed MLC design. Further, it was also intended to have 1 cm projected leaf width at the isocenter. To maintain a symmetry in the field width with respect to central axis (CAX) of the beam, it was required to split the 35 cm field width into two smaller 17.5 cm fields. Accordingly, 34 central and 2 peripheral leaf pairs with projected leaf width of 1 and 0.5 cm, respectively, were chosen. It was also assumed that the MLC leaves were made up of tungsten alloy of density 18.5 g/cm^3. The nomenclature recommended in AAPM Report No. 72 was adopted for describing the different parts of the leaf.[20] Most of the MLC designs, available for linacs, use tongue-and-groove arrangements to assemble the leaves in order to reduce the interleaf leakage. The design of the proposed MLC by Singh *et al.*[11] and Ayyangar *et al.*[12] for telecobalt units also uses a similar concept for assembling the leaves. The effect of underdosing in the region of overlap between two adjacent leaves (which is also called as tongue and groove effect) (Ref. 21) is the main limitation of these two MLC designs for a telecobalt machine. Since the source diameter is about 100 times larger than the interleaf gap ($= 0.2$ mm) of the proposed MLC, a small portion of the total source volume will only be visible through this gap. Due to this partial source view, the magnitude of interleaf leakage of the MLC in a telecobalt machine will be much less. Hence, the tongue and groove free assembling of the MLC leaves was considered in this study.

II.C.1. Reference point for alignment of collimator system

Beam profiles for the field sizes in the range of 5×5 to 35×35 cm^2 defined by jaw type adjustable collimator (for simplicity in the modeling) were generated through Monte Carlo simulation by varying the reference point of alignment. For this purpose, four reference points, namely, (i) center of the source bottom, (ii) center of the source top, (iii) periphery of the source bottom, and (iv) periphery of the source top were selected. The values of field width, radiation beam penumbra, flatness, and symmetry were obtained from these beam profiles and a suitable reference point for alignment of the MLC and x-jaws was selected.

II.C.2. Focusing of the leaf side

Based on the findings of the study described in Sec. II.C.1, the leaf side of the proposed MLC was aligned at the periphery of the source bottom and beam profiles were generated for the nominal mechanical square fields in the range of 6×6 to 35×35 cm^2. Actual radiation field width, F [(lateral separation between 50% dose level at normal treatment distance (NTD)], was determined from these beam profiles. The difference between F and F_n (mechanical field width) was used to determine the correction in the inclination of the leaf side needed to obtain the desired field width. Monte Carlo simulation was repeated by defining the nominal field width using the modified leaf side inclination to confirm the accuracy of the correction.

II.C.3. Leaf end shape

The shape of the leaf end of the proposed MLC is a curved cylindrical surface with the axis of the cylindrical surface perpendicular to the leaf side. Figure 1 shows the dimensional details and location of the MLC leaves with respect to the source bottom. From this geometry, the distance of point T from the central axis where tangent AG touches leaf end, can be given by the following expression:

$$y = r + (38 + h)\tan\emptyset + R\sec\emptyset - R\cos\emptyset. \qquad (1)$$

In Eq. (1), y is the distance of point T from the central axis, r is the radius of the active source ($=1$ cm), R is the radius of curvature of leaf end, $\emptyset$ is the angle between a vertical line parallel to central axis and the tangent drawn to leaf end from the periphery of the source bottom, h is the location of the axis of the cylindrical surface from the top of the leaf. Here, y, r, R, and h are in cm and $\emptyset$ is in degree. For a given field dimension, the divergent optical beam should be tangential to the leaf end and should pass through the periphery of the source bottom (selected reference point). The shape of the leaf end depends on (i) the placement of the axis of the cylindrical surface, and (ii) the radius of curvature. Since variation in the values of h and R can change the leaf end shape, therefore, values of h and R of Eq. (1) were optimized for obtaining required leaf end shape to achieve acceptable field size and penumbra over the entire range of field sizes to be shaped by the MLC of the telecobalt machine.

To optimize the value of h, an arbitrary value of $R = 9.5$ cm was chosen as suggested by Ayyangar *et al.*[12] The beam profiles for 10×10 cm^2 were generated through the Monte Carlo simulation by varying the values of h in the range of 0–7 cm (the leaf height of proposed MLC = 7 cm and hence the maximum value of h = 7 cm). The value of h which produced a radiation field width closer to nominal field width was selected as its optimum value. For optimizing the value of R, a fixed value of h (based on optimization study of h) was selected and beam profiles for 10×10 cm^2 were generated through the Monte Carlo simulation by varying the values of R in the range of 6–15 cm. These beam profiles were analyzed and a reasonable value of R determined.

II.D. X-jaws

The field size along the y-axis (parallel to direction of leaf motion) is defined by the leaf end of the MLC which can have positional resolution of 1 mm. For defining the field size with similar resolution along the x-axis (perpendicular to the direction of leaf motion), a pair of jaw collimator was proposed as an integral component of the MLC. X-jaws of dimension 12 (length) $\times$ 24 (width) $\times$ 5 cm^3 (height) were selected giving due consideration to the range of field sizes to be defined and the leakage and transmitted radiation. The x-jaws were placed below the MLC and the shape of their ends was also optimized similar to as described for the MLC leaf ends.

II.E. Dosimetric characteristics of the MLC

In order to quantify the proposed MLC design, dosimetric characteristics such as radiation field width, beam flatness, symmetry, penumbra, depth dose, and radiation leakage were studied by Monte Carlo simulation. Beam profiles along x-axis (profile across leaf sides/jaw ends) and y-axis (profile across leaf ends) were generated. Radiation field width, penumbra (lateral separation between 80% and 20% dose points on the beam profile, i.e., P80/20), flatness and symmetry (in the flattened region as defined for x-rays from linacs) (Refs. 22–26) were evaluated. For generating the depth dose curves, array of detectors of 1 mm thicknesses along the central axis were defined in the simulation with 80 cm SSD.

II.F. Transmission and leakage through the MLC

To determine the inter- and intraleaf transmission though the MLC, the method used by various other authors[27–30] was adopted. In this study, field defining jaws were either completely open or completely closed. The array of voxels, each of volume 0.72 cm^3, along the x-axis (perpendicular to leaf motion) at 0.5 cm depth and 79.5 cm SSD were used to score the energy deposited per source particle. The MLC leaves were closed 10 cm away from the central axis (i.e., at an offaxis distance of 10 cm) keeping x-jaws completely open. Peak dose rate under reference condition was quantified by recording the energy deposited in the central voxel. Percentage radiation transmission was calculated by taking the ratio of the energy deposited in a voxel and the peak dose rate under reference condition.

The leakage radiation between leaf ends was determined under two different conditions. In the first case, leaves were closed on the central plane (plane containing the central axis) keeping the x-jaws fully opened and the energy deposited in the array of voxels along the y-axis (parallel to leaf motion) was scored. In the second case, the leaves were closed at 10 cm away from the central plane keeping the x-jaws fully opened and the energy deposited in the array of voxels along the y-axis was scored. Percentage radiation transmission was calculated by taking the ratio of the energy deposited in a voxel and the peak dose rate under reference condition.

III. RESULTS AND DISCUSSIONS

III.A. Benchmarking of the simulation

The Monte Carlo simulation was benchmarked by comparing experimentally measured dosimetry data of the Bhabhatron-II telecobalt machine to Monte Carlo generated data. Figure 2 shows MCNP generated and experimentally measured beam profiles at d$_m$ and 5 cm depths for 10×10 cm^2 field from Bhabhatron-II telecobalt machine. It can be seen that the MCNP generated and measured beam profiles are in good agreement to each other. The MCNP generated, experimentally measured and BJR (Ref. 31) percentage depth dose (PDD) data were also found to be in good
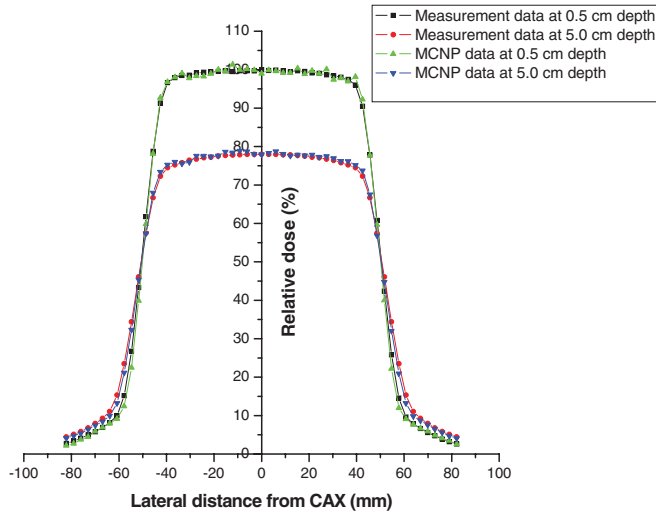
FIG. 2. MCNP generated and experimentally measured beam profiles of Bhabhatron-II telecobalt machine at the depths of dose maximum (d_m) and 5 cm for 10×10 cm^2 field size.

FIG. 3. MCNP generated beam profiles at d_m for 10×10 cm^2 field size with varying reference point of alignment of adjustable collimator for a telecobalt machine.

agreement to one another. These results confirm the suitability and accuracy of our Monte Carlo simulation method.

III.B. Reference point for alignment of collimator system

Figure 3 shows beam profiles at d_m for 10×10 cm^2 field for four different reference points selected for the alignment of the adjustable collimator. The beam profiles were generated for the field sizes in the range of 5×5 to 35×35 cm^2; however, the beam profiles are only shown for 10×10 cm^2 field size for clarity in the presentation. The values of field width, beam penumbra, flatness, and symmetry obtained from these profiles are shown in Table I. On analyzing the data in Table I, it is observed that the dosimetric parameters with reference point at the periphery of the source bottom and at the periphery of the source top are within the acceptable values.[22–26] This may be due to the fact that when the reference point for alignment is taken at the periphery of the source bottom/top, almost all the entire source is visible from all field sizes. However, when the reference point for alignment is taken at the center of the source bottom/top, only part
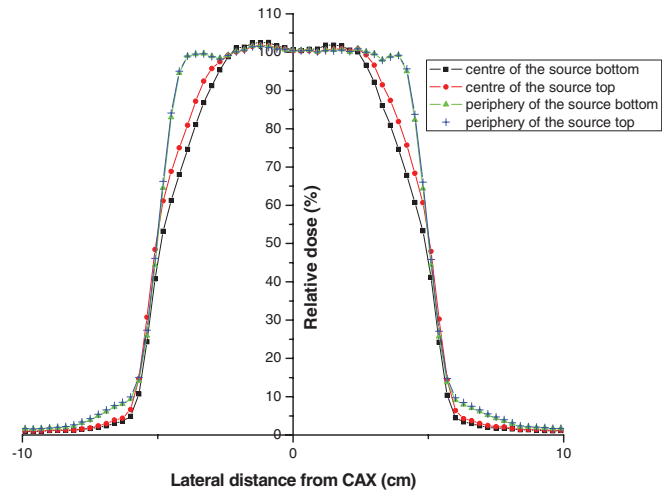
of the source is visible and the visible size of the source is field size dependent. Since the top of the active ^{60}Co source varies with the source strength for a given specific activity, the periphery of the source bottom can be considered as the most suitable reference point for alignment of the adjustable collimator. Accordingly, the periphery of the source bottom was taken as the reference point for alignment of the ends and sides of the proposed MLC. Specifically, two reference points at the periphery of the source bottom, 180° apart from each other, were chosen as the reference points for focusing of the ends and sides of the MLC. This result is similar to that from Mora *et al.*[32] where they selected the inner corner of the top of the primary collimator for pivoting the adjustable collimator of the telecobalt machine. Unlike the small focal spot size ($\sim$ point source) in linac,[33] the ^{60}Co source in a telecobalt machine has a finite volume.[9] The location of the reference point for alignment (focusing point) of the MLC is very critical.

III.C. Focusing of the leaf side

Figure 4 shows the schematic diagram of the inclination of leaf side of MLC with respect to the CAX. The leaves A and B are the opposing MLC leaves, the side of which is

TABLE I. Beam characteristics with varying reference point of alignment of jaw type collimator.

| Field size (cm^2) | Beam characteristics for reference point of alignment at | | | | | | | | | | | |
| | Bottom of the source center | | | Top of the source center | | | Periphery of the source bottom | | | Periphery of the source top | | |
	Flat. (%)	Sym. (%)	Pen. (mm)	Flat. (%)	Sym. (%)	Pen. (mm)	Flat. (%)	Sym. (%)	Pen. (mm)	Flat. (%)	Sym. (%)	Pen. (mm)
5×5	23.83	0.49	24.0	12.57	0.51	16.66	1.27	0.31	9.18	1.33	0.38	9.40
10×10	18.07	0.48	20.24	13.0	0.51	16.66	2.56	0.07	9.98	3.01	0.01	14.06
15×15	10.88	0.24	26.52	7.42	0.36	17.98	2.88	0.32	13.4	2.98	0.03	16.4
20×20	7.12	0.17	26.50	4.74	0.19	18.54	2.97	0.15	15.7	2.82	0.42	15.88
25×25	5.11	0.10	28.51	4.20	0.11	19.02	2.95	0.06	14.35	3.02	0.79	15.46
30×30	4.86	0.06	29.88	4.52	0.09	21.05	2.59	0.04	15.69	2.91	0.34	16.43
35×35	1.57	1.35	28.69	5.17	0.32	20.3	3.01	0.09	15.73	3.04	0.51	19.43
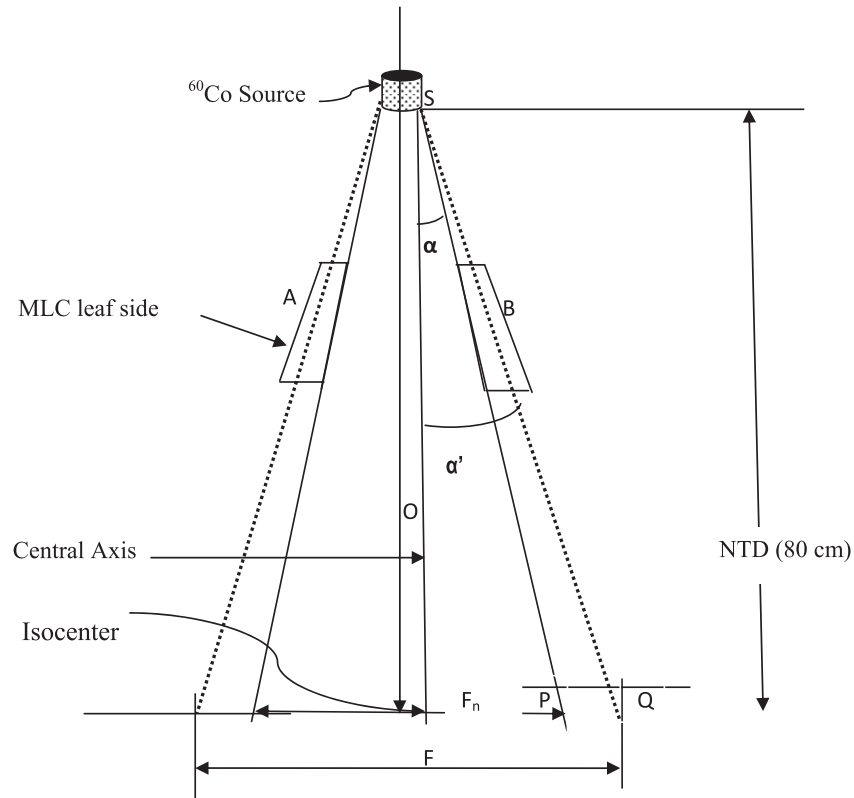
FIG. 4. Alignment of leaf sides of MLC for obtaining desired field width (F_d) from the nominal mechanical field width (F_n). F is the actual radiation field width corresponding to nominal mechanical field width F_n and the difference (F−F_n) is the error (ΔF) in the nominal mechanical field width and actual radiation field width. Ideally, $F_n = F_d$.

focused at the periphery of the source bottom. α and α' are the angles between the leaf side and the line parallel to the CAX corresponding to nominal mechanical field width (F_n) and its radiation field width (F). The difference ΔF ($= F - F_n$) indicates the error in the nominal mechanical field width and its radiation field width. Table II presents the parameters of the nominal mechanical field width and its radiation field width and the estimated reduction in inclination in leaf side $\Delta\alpha$ ($= \alpha' - \alpha$) with respect to the line parallel to the CAX for obtaining desired radiation field width. The average reduction in inclination of the leaf side corresponding to field error ΔF was found to be 0.56°. Table III shows the modified inclination (θ) of the leaf side with respect to the line parallel to the central

axis for obtaining desired radiation field width (F_d). The radiation field width (L) from the beam profiles generated using MCNP is also shown in this table. It can be observed from this table that F_d and L are comparable to each other within the permissible tolerance limits[22–26] which in turn verifies that the modified inclination of leaf side provides desired radiation beam.

III.D. Leaf end shape

A plot of radiation field width versus h is shown in Fig. 5. This variation of radiation field width is useful in choosing an optimum value of h. It can be seen from this figure that at

TABLE II. Parameters of the nominal mechanical field width and its radiation field width. α and α' are the angles between leaf side and the line parallel to the central axis (CAX) corresponding to nominal mechanical field (F_n) and actual radiation field (F), respectively. $\Delta\alpha$ ($= \alpha' - \alpha$) is the reduction in inclination of leaf side with respect to the line parallel to the CAX for obtaining desired radiation field width (F_d).

Nominal mechanical field (F_n)		Actual radiation field (F) corresponding to F_n		Field error	$\Delta\alpha$ ($= \alpha' - \alpha$)
Width (cm)	α (deg)	Width (cm)	α' (deg)	[$\Delta F = (F - F_n)$] (cm)	(deg)
6	1.44	7.65	2.02	1.65	0.58
10	2.86	11.55	3.42	1.55	0.56
14	4.29	15.52	4.85	1.52	0.56
20	6.42	21.51	6.98	1.51	0.56
24	7.83	25.41	8.39	1.41	0.56
30	9.93	31.30	10.48	1.30	0.55
35	11.65	36.30	12.19	1.30	0.54

TABLE III. Estimated inclination (θ) of leaf side with respect to the line parallel to the central axis for obtaining desired radiation field width (F_d). L is the measured radiation field width from MCNP generated beam profile.

F_d (cm)	θ (deg)	L (cm)
6	0.86	6.17
10	2.30	10.06
14	3.73	14.05
20	5.86	19.95
24	7.27	23.90
30	9.38	29.90
35	11.11	34.95

$h = 5$ cm (for $R = 9.5$ cm), the difference between radiation field width and mechanical field width across leaf ends is minimum (=1.72 cm). For the same mechanical field width, the difference between radiation field width and mechanical field width across leaf sides is 1.55 cm (see Table II). This indicates that at $h = 5$ cm, radiation field widths across leaf ends and leaf sides are comparable. Thus, 5 cm was taken as the optimum value of h. It is to be noted that the objective of the optimization of the leaf end shape was to obtain radiation field width across leaf ends comparable to radiation field width across leaf sides for a given mechanical field so that changing the inclination of the leaf sides by a fixed value could make the radiation and mechanical field comparable within the given tolerance of 2 mm. In view of this requirement, the magnitude of the difference between radiation and mechanical field width is insignificant.
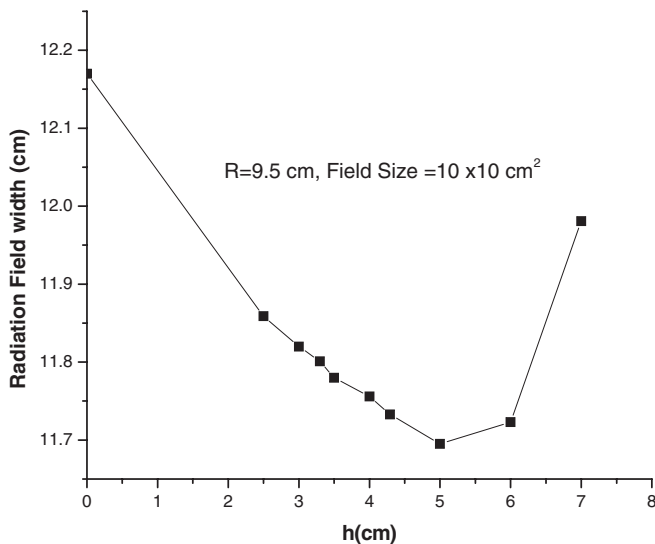
The optimization study of R indicated that varying the radius of curvature of the leaf end did not affect the radiation field width appreciably. For $R = 9.5$ cm ($h = 5$ cm), the difference in radiation and mechanical field width was found to be within the acceptable tolerance of 0.2 cm for field sizes up to 24×24 cm^2. For field sizes larger than 24×24 cm^2, this difference was higher than the acceptable tolerance values. Since the difference between the radiation and mechanical field width for $R = 9.5$ cm was not within the acceptable tolerance limit for the entire range of field sizes, the simulation was repeated by arbitrarily reducing the value of R. For $R = 8$ cm, the difference in radiation and mechanical field width was found to be within acceptable tolerance of 0.2 cm for all field sizes. Thus, 8 cm was taken as optimized value of R for characterizing the MLC.

III.E. X-jaws

A plot of radiation field width, corresponding to nominal mechanical field size of 10×10 cm^2, versus h_x (location of the axis of the curved ends of x-jaws from its top) for x-jaws is shown in Fig. 6. This variation of radiation field width is useful in choosing an optimum value of h_x. It can be seen from this figure that at $h_x = 0$ cm the radiation field width across x-jaws is relatively closer to radiation field width across leaf sides. However, to obtain radiation field width across x-jaws further closer to radiation field width across leaf sides, it is required to modify the end shape of x-jaws by varying R_x (radius of curvature of ends of x-jaws). It was observed that varying the radius of curvature of the x-jaw end does not affect the radiation field width appreciably as observed in the case of leaf end. A value of $R_x = 6$ cm was chosen to obtain radiation

FIG. 5. Variation of radiation field width along y-axis (across leaf ends) as a function of h (location of the axis of the cylindrical surface from the top of the leaf). This variation of radiation field width is useful in choosing an optimum value of h. Radiation field widths were determined at 50% dose values of the profiles generated at d_m (SSD = 79.5 cm) varying the value of h for a given mechanical field of 10×10 cm^2 and radius of curvature of leaf ends, $R = 9.5$ cm. For a given mechanical field of 10×10 cm^2, the value of radiation field width across the leaf ends was found closer to that of radiation field width across the leaf sides for $R = 9.5$ cm and $h = 5$ cm.
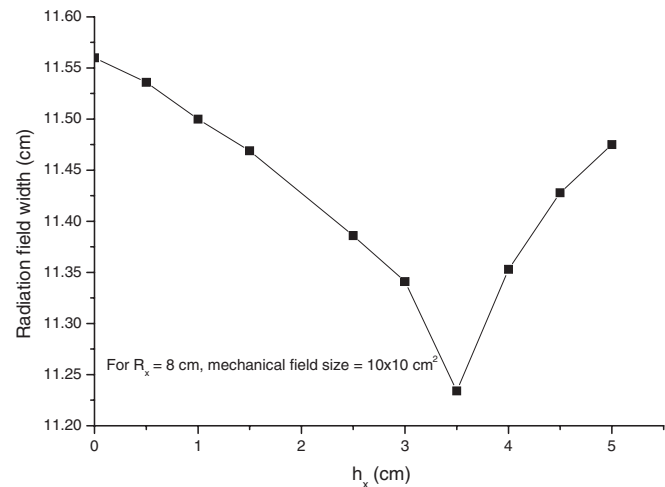

FIG. 6. Variation of radiation field width along x-direction (defined by x-jaws) as a function of h_x (location of the axis of the curved ends of x-jaws from its top). This variation of radiation field width helps in choosing an optimum value of h_x. Radiation field widths were determined at 50% dose values of the profiles generated at d_m (SSD = 79.5 cm) varying the value of h_x for a given mechanical field of 10×10 cm^2 and radius of curvature of ends of x-jaws, $R_x = 8$ cm. For a given mechanical field of 10×10 cm^2, the value of radiation field width across the ends of x-jaws was found closer to that of radiation field width across the leaf sides for $R_x = 8$ cm and $h_x = 0$ cm.
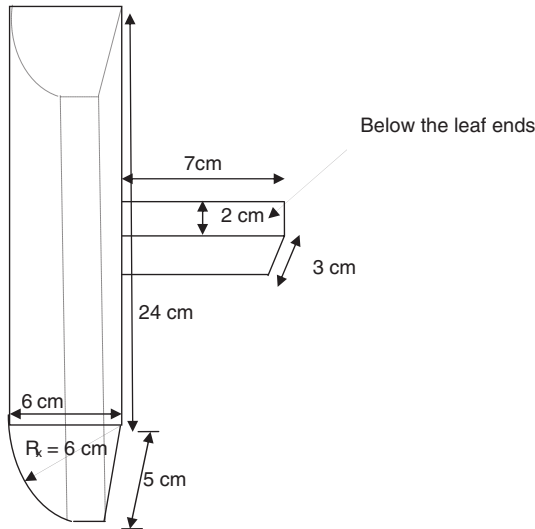
FIG. 7. Schematic diagram showing modified design of the x-jaw having 6 cm length, 24 cm width, and 5 cm height with rounded end shape (R_x = 6 cm, h_x = 0) toward the central axis. It also contains a block of 7 cm length, 2 cm width, and 3 cm height for reducing the leaf end leakage.

field width comparable to radiation field width across the leaf sides over the entire range of field sizes within tolerance value of 0.2 mm.

The collimating jaws can be placed either above or below the proposed MLC. When the x-jaws are placed above the MLC, jaws of relatively smaller lengths and widths are required which may be economical and will require a leaf motor of relatively smaller torque. The overall mechanical weight of the collimating system will also likely be less. However, placing the x-jaws above the MLC may give rise to relatively larger penumbra because of the shorter distance from the source. When the x-jaws are placed below the MLC, jaws of relatively larger lengths and widths will be required which may not be economical and will require a motor of relatively larger torque. The overall mechanical weight of the collimating system will also increase. However, this option of placing the x-jaws below the MLC may give rise to relatively smaller
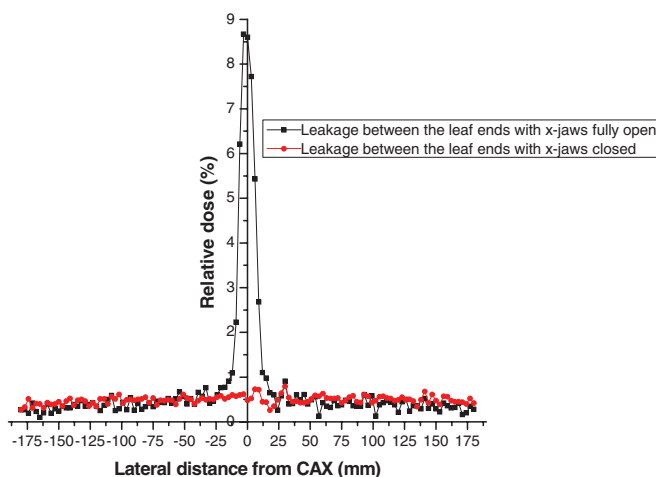
penumbra because of the larger distance from the source. In both situations, an optimized end shape (similar to leaf end shape) jaws are required.

Further, from Sec. III.G it is clear that the leakage from the MLC (through the leaf and between the leaves) with x-jaws completely opened is well below the permissible values.[34,35] It is to be noted that while defining a field length using x-jaws along x-axis, an extra pair of leaves are kept open at the field boundary to avoid interference of the leaf side with the x-jaws and rest of the leaves that are closed. The leakage between the leaf ends in closed condition is 8.6%. This needs to be reduced to permissible limit[34,35] using the x-jaws located below the MLC. To fulfill this requirement, 3 cm height and 2 cm width of x-jaws are found adequate to bring down the leakage through the leaf ends to within acceptable values. A modified x-jaw, 5 cm height, 24 cm width, and 6 cm length with rounded end toward the central axis was adopted. It also contains a block of 7 cm length, 2 cm width, and 3 cm height for reducing the leaf end leakage. The modified design of the x-jaw is shown in Fig. 7. The overall weight of the modified x-jaws has appreciably been reduced which will require a motor of relatively lesser torque. The percentage leakage through the leaf ends when x-jaws are open and closed are shown in Fig. 8. The maximum and average leakage through the leaf ends with x-jaws closed is 0.78% and 0.48%, respectively. Hence, it is observed that leakage through the leaf ends are comparable to leakage through the MLC when x-jaws are closed and the values are well below the International Electrotechnical Commission (IEC) recommended values.[34,35]

III.F. Dosimetric characteristics of MLC

Figure 9 shows the MCNP plot of vertical cross section of the proposed MLC along with x-jaws. The leaves and jaws are shown here in the closed condition for clear illustration of the mechanical arrangements. Table IV presents the dosimetric parameters of the MLC. It can be observed from Table IV that the penumbra is in the range of 8.89–12.71 mm over the entire range of field sizes for the proposed MLC which is well below its commonly acceptable value. Thus, the challenge of achieving a smaller radiation beam penumbra without the use

FIG. 8. Percentage leakage through leaf ends when x-jaws are (i) completely open, and (ii) closed at an offaxis of 10 cm.
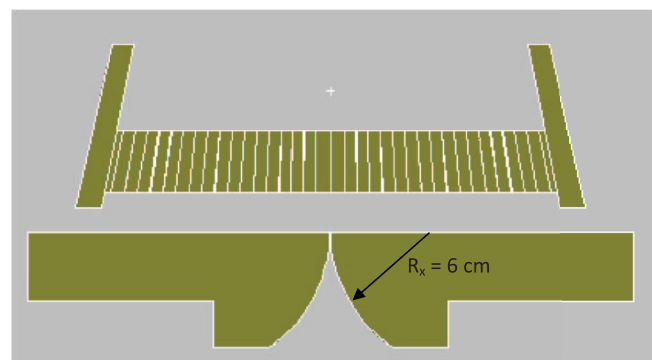

FIG. 9. MCNP plot of the vertical cross section of the proposed MLC along with x-jaws for a telecobalt machine. Leaves and jaws are shown in closed condition for clear demonstration of the mechanical arrangements.

TABLE IV. Dosimetric parameters of Monte Carlo simulated beam profiles at dm defined by x-jaws, sides and ends of the MLC.

Field size (cm^2)	Dosimetric parameters for fields defined by											

	x-jaws (x-axis)				Leaf sides (x-axis)				Leaf ends (y-axis)			
Field size (cm^2)	RFW (cm)	F (%)	S (%)	P (mm) P_L/P_R	RFW (cm)	F (%)	S (%)	P (mm) P_L/P_R	RFW (cm)	F (%)	S (%)	P (mm) P_L/P_R
6 × 6	5.95	0.60	0.02	8.89/ 9.25	6.10	1.01	0.04	9.99/ 10.20	6.09	1.78	0.39	10.25/10.01
10 × 10	10.01	2.19	0.08	10.04/10.07	10.09	2.72	0.06	10.59/10.72	10.06	2.56	0.03	10.45/10.18
14 × 14	13.88	2.88	0.03	9.63/ 9.95	14.05	2.68	0.01	10.98/10.96	14.05	2.29	0.10	10.83/10.44
20 × 20	19.94	2.32	0.05	10.17/ 10.12	19.98	2.79	0.08	11.32/11.16	20.07	2.64	0.05	11.02/10.66
24 × 24	23.82	2.43	0.28	9.92/ 10.03	23.93	2.58	0.00	11.33/11.23	24.07	1.94	0.12	11.01/11.14
30 × 30	29.95	2.83	0.10	10.37/ 10.44	29.86	2.56	0.03	11.57/11.74	30.19	2.99	0.12	12.08/ 12.03
35 × 35	34.96	3.07	0.06	11.08/ 10.97	34.79	3.41	0.05	11.72/12.16	35.28	3.51	0.14	12.01/12.71

Note: RFW is the radiation field width measured at 50% dose levels; F and S are beam flatness and symmetry, respectively; and P is the 80-20 penumbra measured at left (P_L) and right (P_R) sides of beam profile.

of the trimmer bars is met. It is also observed from Table IV that the values of all the dosimetric parameters including radiation field width are well within the permissible tolerance over the entire range of field sizes.

Table V presents the values of d_m and percentage depth dose at 10 cm (D_{10}) recorded from the depth dose curves generated through Monte Carlo simulation along with BJR (Ref. 32) data. Relative surface dose at 0.5 mm depth recorded from the depth dose curves as per IEC definition[36] is also listed in this table. As per IEC recommendation, the relative absorbed dose at 0.5 mm depth (D_s) on the radiation beam axis for a telecobalt machine with 80 cm NTD shall not exceed 70% and 90% of absorbed dose at 5 mm depth for 10 × 10 and 35 × 35 cm^2 field size, respectively. From Table V it can be seen that the value of D_s for 10 × 10 cm^2 and 35 × 35 cm^2 are 41.54% and 44.86%, respectively, which are well below the IEC recommended values. Depth of maximum dose was observed to be 0.5 cm for field sizes up to 24 × 24 cm^2 and thereafter reduces to 0.4 cm, because of increase in electron contamination. However, BJR data show the same value of depth of maximum dose irrespective of field sizes. Percentage depth dose at 10 cm depth (D_{10}) of the MLC is also given in Table V along with BJR data. The difference between MCNP calculated values and BJR data of D_{10} is less that 1%.

Radiation beam penumbra is a major concern in a telecobalt machine because of the relatively large physical size of the source (typically it ranges from 1.5 to 2.0 cm in diameter) (Ref. 9) in comparison to the focal spot size in a medical linac (typical focal spot size is about 2 mm diameter).[19] The radiation beam penumbra mainly depends on the source size, distance between the source and the end of the collimating system, shape and alignment of the side of the collimating system facing the beam divergence. Trimmers are usually employed to reduce the radiation beam penumbra in a telecobalt machine, which has either jaw type or multivane collimator. However, employing the penumbra trimmers will not be possible with a telecobalt machine incorporating a MLC. The available options for reducing penumbra in a MLC equipped telecobalt machine would be to use either a ^{60}Co source of smaller diameter or increase the distance between the source and the end of the collimating system. However, to maintain the same source strength with a smaller diameter, the height of the source will need to be increased for a given specific activity. The increase in the height of source will lead to self-absorption causing reduction in absolute dose rate (output) of the machine.[20] Hence, increasing the distance between source and the collimating system is the only option left for reducing the beam penumbra from a telecobalt machine. A distance of 45 cm between the source and the MLC was chosen.

TABLE V. A comparison of relative surface dose (D_s), depth of dose maximum (d_m), and percentage depth dose at 10 cm depth (D_{10}) of the proposed MLC with BJR data.

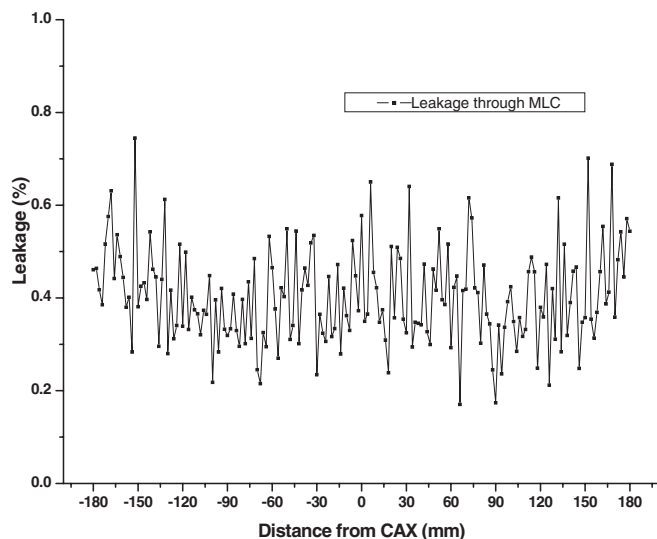| Field size (cm^2)	D_s (%)	d_m (cm)		D_{10} (%)		
	MCNP	MCNP	BJR	MCNP	BJR	Difference in MCNP and BJR values (%)
6 × 6	38.78	0.5	0.5	52.3	52.5	0.38
10 × 10	40.02	0.5	0.5	55.9	56.4	0.89
14 × 14	40.94	0.5	0.5	60.4	59.2	− 2.03
20 × 20	41.68	0.5	0.5	61.4	60.8	− 0.99
24 × 24	41.68	0.5	0.5	61.6	61.9	0.48
30 × 30	43.05	0.4	0.5	62.1	62.6	0.80
35 × 35	44.86	0.4	0.5	63.0	63.2	0.32

FIG. 10. Percentage leakage through the MLC when leaves were closed 10 cm away from the central axis keeping x-jaws completely open. The percentage leakage was calculated relative to dose rate for 10×10 cm^2 field at d_m. The peaks are due to interleaf leakage.

III.G. Radiation leakage

Percentage leakage through the MLC, when the leaves were closed 10 cm away from the CAX but keeping x-jaws completely open, is shown in Fig. 10. The peaks of this curve are due to interleaf leakage resulting from the air gap between the leaf sides. Permissible leakage radiation through beam limiting devices (BLDs) comprising either single element (e.g., jaw collimator) or multielements (e.g., MLC) in the patient plane has been recommended by IEC.[34,35] As per the current IEC recommendations, the maximum and average values of leakage radiation through BLDs including MLCs shall not exceed 2% and 0.75%, respectively, of peak dose rate under reference condition (at d_m along central axis for 10×10 cm^2 field with SSD of 79.5 cm). The maximum and average radiation leakage through the MLC is 0.74% and 0.41%, respectively, which are well below the permissible leakage level recommended by the IEC. Percentage leakage through leaf ends when leaves were closed on CAX keeping x-jaws completely open is shown in Fig. 8. The percentage leakage through the leaf ends is 8.6% and 2.3% when leaves were closed at CAX and 10 cm offaxis, respectively. Thus, the leakage through the leaf ends from the proposed MLC is far less than the leakage through the leaf ends of commercially available MLCs for linacs (13.5%–27.4%).[27] This is probably because the telecobalt machine has inherently low leakage due to partial source view.

IV. CONCLUSIONS

A secondary multileaf collimator has been proposed for a telecobalt machine of NTD 80 cm. Initially, a basic design of the MLC was selected and its various characteristics including dosimetry parameters, leakage, effect of reference point of alignment, and the shape of the leaf ends and sides were studied. Monte Carlo simulations were carried out to optimize the

shape of the leaves ends and the jaws. The periphery of the source bottom was found to be the most suitable location for alignment of the MLC. An optimized version of the MLC was proposed which contains an optimized shape of ends of leaves and the jaws. The MLC assembly consisting of leaves and jaws are capable of defining field size in steps of 0.1 cm along two major axes (i.e., x-axis and y-axis) up to 35×35 cm^2. The dosimetry parameters (beam flatness, beam symmetry, radiation beam penumbra, depth dose, and surface dose) of this MLC were found to be well within their recommended tolerances. The average and maximum leakage through the MLC were also found to be well below the IEC recommended values. The proposed MLC can be potentially integrated to any telecobalt machine of NTD 80 cm by replacing the adjustable collimator with the proposed MLC assembly. The integration of the MLC with telecobalt unit will enable this machine to be used as a conformal radiotherapy device.

[a] Author to whom correspondence should be addressed. Electronic mail: gsahani@gmail.com/gsahani@aerb.gov.in; Telephone: +91-22-25990653; Fax: +91-22-25990650.

[1] C. Fox, H. E. Romeijn, L. Bart, C. Men, D. M. Aleman, and J. F. Dempsy, "Comparative analysis of ^{60}Co intensity-modulated radiation therapy," Phys. Med. Biol. **53**, 3175–3188 (2008).

[2] C. P. Joshi, S. Dhanesar, J. Darko, A. Kerr, P. B. Vidyasagar, and J. L. Schreiner, "Practical and clinical considerations in Cobalt-60 tomotherapy," J. Med. Phys. **34**(3), 137–140 (2009).

[3] J. L. Schreiner, C. P. Joshi, J. Darko, A. Kerr, G. Salomons, and S. Dhanesar, "Role of Cobalt-60 in modern radiation therapy: Dose delivery and image guidance," J. Med. Phys. **34**(3), 133–136 (2009).

[4] P. Cadman and K. Bzdusek, "Co-60 tomotherapy: A treatment planning investigation," Med. Phys. **38**(2), 556–564 (2011).

[5] P. Cadman, "An investigation of beam parameters for Co-60 tomotherapy," Med. Phys. **34**(10), 3838–3843 (2007).

[6] E. J. Adams and A. P. Warrington, "A comparison between cobalt and linear accelerator-based treatment plans for conformal and intensity-modulated radiotherapy," Br. J. Radiol. **81**, 304–310 (2008).

[7] G. Sahani, M. Kumar, P. K. Dash Sharma, D. N. Sharma, K. Chhokra, B. Mishra, S. P. Agarwal, and R. K. Kher, "Compliance of Bhabhatron-II telecobalt unit with IEC standard - Radiation safety," J. Appl. Clin. Med. Phys. **10**(2), 120–130 (2009).

[8] P. Matcalfe, T. Kron, and P. Hoban, *The Physics of Radiotherapy X-Rays from Linear Accelerators* (Medical Physics Publishing, Madison, WI, 1997).

[9] F. M. Khan, *The Physics of Radiation Therapy*, 4th ed. (Lippincott, Baltimore, 2010).

[10] D. C. Kar, K. Jayarajan, S. D. Sharma, M. Singh, and G. V. Subrahmanyam, "The Bhabhatron: An affordable solution for radiation therapy," Biomed. Imaging Interv. J. **4**(4), e50–12 (2008).

[11] I. R. R. Singh, B. P. Ravindran, and K. M. Ayyangar, "Design and development of motorized multileaf collimator for telecobalt unit," Technol. Cancer Res. Treat. **5**(6), 597–605 (2006).

[12] K. M. Ayyangar, M. D. Kumar, P. Narayan, F. Jesuraj, and M. R. Raju, "Monte Carlo simulation of a mutli-leaf collimator for telecobalt machine using BEAMnrc code," J. Med. Phys. **35**(1), 23–32 (2010).

[13] J. F. Briesmeister, "MCNP-A general Monte Carlo N-Particle transport code, Version B," Report No. LA-12625-M (Los Alamos National Laboratory, Los Almos, 1997).

[14] J. K. Shultis and R. E. Faw, *An MCNP Primer* (Kansas State University, Manhattan, 2006).

[15] B. T. Sichani and M. Sohrabpour, "Monte Carlo dose calculations for radiotherapy machines: Theratron 780-C teletherapy case study," Phys. Med. Biol. **49**, 807–818 (2004).

[16] R. Miro, J. Soler, S. Gallardo, J. M. Campayo, S. Diez, and G. Verdu, "MCNP simulation of a Theratron 780 radiotherapy unit," Radiat. Prot. Dosim. **116**(1–4), 65–68 (2005).

[17] R. Miro, B. Juste, S. Gallardo, A. Santos, and G. Verdu, "Cobalt therapy dosimetric calculations over a voxelized heterogeneous phantom: Validation of different Monte Carlo models and methodologies against experimental data," IEEE Trans. Nucl. Sci. **53**(6), 3808–3817 (2006).

[18] R. G. Jain, R. Kushwaha, and K. V. S. Sastry, "Teletherapy sources with imported and indigenous ^{60}Co activity," J. Med. Phys. **34**(3), 180–181 (2009).

[19] C. P. Joshi, J. Darko, P. B. Vidyasagar, and L. J. Schreiner, "Investigation of an efficient source design for Cobalt-60 based tomotherapy using EGSnrc Monte Carlo simulations," Phys. Med. Biol. **53**, 575–592 (2008).

[20] American Association for Physicists in Medicine, "Basic applications of multileaf collimators," AAPM Report No. 72 (Task Group No. 50) (AAPM, College Park, MD, 2001).

[21] S. D. Sharma, E. Cassani, C. Mordacchini, R. Mantovani, R. Novario, L. Conte, and B. C. Bhatt, "Tongue and groove effect of Varian MLC for different clinical conditions," J. Med. Phys. **29**(2), 48–54 (2004).

[22] International Electrotechnical Commission, "Medical electrical equipment; Medical electron accelerators- Functional performance characteristics," Report No. IEC-60976 (IEC, Geneva, 2000).

[23] International Atomic Energy Agency, "Setting up a radiotherapy programme: Clinical, medical physics, radiation protection and safety aspects," Report No. STI/PUB/1296 (IAEA, Vienna, 2008).

[24] G. J. Kutcher, L. Coia, M. Gillin, W. F. Hanson, S. Leibel, J. M. Morton, J. R. Palta, J. A. Purdy, L. E. Reinstein, G. K. Svensson, M. Weller, and L. Wingfield, "Comprehensive QA for Radiation Oncology: Report No. 46 of AAPM Radiation Therapy Committee Task Group No. 40," Med. Phys. **21**(4), 581–618 (1994).

[25] Netherlands Commission on Radiation Dosimetry, "Quality control of medical linear accelerator: Current practice and minimum requirements," Report No. 9 (NCS, Delft, The Netherlands, 1996).

[26] R. Nath, P. J. Biggs, F. J. Bova, C. C. Ling, J. A. Purdy, J. van de Gein, and M. S. Weinhous, "AAMP code of practice for radiotherpay accelerators: Report of AAPM Radiation Therapy Committee Task Group No. 45," Med. Phys. **21**, 1093–1121 (1994).

[27] M. B. Tacke, S. Nill, P. Haring, and U. Oelfke, "6 MV dosimetric characterization of the 160 MLC^{TM}, the new Siemens multileaf collimator," Med. Phys. **35**(5), 1634–1642 (2008).

[28] J. O. Kim, J. V. Siebers, P. J. Keall, M. R. Arnfield, and Radhe Mohan, "A Monte Carlo study of radiation transport through multileaf collimators," Med. Phys. **28**(12), 2497–2506 (2001).

[29] M. S. Huq, I. J. Das, T. Steinberg, and J. M. Galvin, "A dosimetric comparison of various multileaf collimators," Phys. Med. Biol. **47**, 159–170 (2002).

[30] T. Yamamoto, T. Teshima, S. Yano, M. Matsumoto, Y. Nagata, and M. Hiraoka, "Monte Carlo calculation of leakage radiation through the multileaf collimator," in *Proceedings of the Tenth EGS4 Users' Meeting in KEK, Tsukuba, Japan*, *KEK Proceedings* Vol. 18 (KEK, Radiation Science Centre, Tsukuba, 2002), pp. 84–88.

[31] British Institute of Radiology, "Central axis depth dose data for use in radiotherapy," Br. J. Radiol. (Suppl. 25) (1996).

[32] G. M. Mora, A. Maio, and D. W. O. Rogers, "Monte Carlo simulation of a typical ^{60}Co therapy source," Med. Phys. **26**(11), 2494–2502 (1999).

[33] P. Munro, J. A. Rawlinson, and A. Fenster, "Therapy imaging: Source sizes of radiotherapy beams," Med. Phys. **15**, 517–524 (1988).

[34] International Electrotechnical Commission, "Part 2-1: Particular requirements for the safety of electron accelerators in the range 1 MeV to 50 MeV," Report no. IEC-60601-2-1 (IEC, Geneva, 1998).

[35] International Electrotechnical Commission, "Part2-1: Particular requirements for the safety of electron accelerators in the range 1 MeV to 50 MeV," Report No. IEC-60601-2-1 (Amendment 1) (IEC, Geneva, 1998).

[36] International Electrotechnical Commission, "Part2: Particular requirements for the safety of gamma beam therapy equipment," Report No. IEC-60601-2-11 (IEC, Geneva, 1997).